Materials Research Express

PAPER • OPEN ACCESS

Electronic properties and crystal structures of double-perovskites, $Ba_2Bi^{III}Bi^{V}O_6$,Ba_2PrBiO_6, and Ba_2PrSbO_6: First-principles study

Materials Research Express

PAPER

Electronic properties and crystal structures of double-perovskites, $Ba_2Bi^{III}Bi^{V}O_6$,Ba_2PrBiO_6, and Ba_2PrSbO_6: First-principles study

Kazume Nishidate[1], **Achy Adiko**[1], **Michiaki Matsukawa**[1], **Haruka Taniguchi**[1], **Arisa Sato**[1], **Akiyuki Matsushita**[2], **Satoru Tanibayashi**[3] **and Masayuki Hasegawa**[4]

[1] Faculty of Science and Engineering, Iwate University, Morioka 020-8551, Japan
[2] National Institute for Materials Science, Ibaraki 305-0047, Japan
[3] Department of Engineering for Future Innovation, National Institute of Technology, Ichinoseki College, Ichinoseki 021-8511, Japan
[4] Professor Emeritus, Iwate University, Morioka 020-8550, Japan

E-mail: nisidate@iwate-u.ac.jp

Keywords: double-perovskite, band structure, hybrid functional

OPEN ACCESS

RECEIVED
17 March 2020

REVISED
26 May 2020

ACCEPTED FOR PUBLICATION
29 May 2020

PUBLISHED
10 June 2020

Abstract

In recent experiments, a significant band gap widening was observed when Sb was substituted for Bi in the double-perovskite Ba_2PrBiO_6. In this work, we study a series of double-perovskites, $Ba_2Bi^{III}Bi^{V}O_6$, Ba_2PrBiO_6, and Ba_2PrSbO_6 using the first-principles density functional theory with the Heyd-Scuseria-Ernzerhof hybrid functional to investigate the substitution effect on the structural and electronic properties. We find that the two topmost valence bands are disappeared on the substitution of Pr^{III} for Bi^{III}, and the two bottommost conduction bands are disappeared on the substitution of Sb^{V} for Bi^{V}, causing the significant band gap widening. Further, our calculation suggests that the $Ba_2PrPr_{Bi}O_6$ is a possible candidate as a source of the Pr^{IV} signal observed in the experiment. We find that the *B*-site disordering atomic configuration, $Ba_2B''^{V}B'^{III}O_6$, are restored to those of the original structures. On the other hand, our results also suggest the importance of the partial *B*-site disorder to explain the experimentally observed band gaps.

1. Introduction

TiO_2 is well known as an efficient photo catalytic material and has a wide range of application area from air-purifier to antimicrobial coating [1–6]. However, TiO_2 uses only the ultraviolet ray which is less than 3% of the whole sunlight pouring on the Earth surface. Therefore extensive studies have been devoted to develop photo-catalytic materials sensitive to visible light that makes up 50% of the sunlight. A large number of double-perovskite oxides, $A_2B'^{III}B''^{V}O_6$, have been studied due to their intriguing physical and chemical properties originating in their mixed valence nature [7]. Above all, Ba_2PrBiO_6 was found to show an efficient photo catalytic activity to dissolve water molecules into oxygen and hydrogen gases under the visible light [8, 9]. Recent experiment on the Ba_2PrSbO_6 suggests the presence of the typical *B*-site ordering and the band gap modification [10, 11]. However, detailed theoretical analysis on the electronic structures and the crystal geometries of the double-perovskites has not been performed. In this work, we study the structural and electronic properties of $Ba_2Bi^{III}Bi^{V}O_6$, Ba_2PrBiO_6, and Ba_2PrSbO_6 double-perovskites using the first-principles density functional theory. The Heyd-Scuseria-Ernzerhof hybrid functional was applied to the calculations to handle the strong electron-correlation. We find that the Bi^{III} 6s states at the top of valence band of $Ba_2Bi^{III}Bi^{V}O_6$ vanish on the Pr substitution for Bi at B'^{III}-site. When Sb is substituted for Bi at B''^{V}-site, the Bi^{V} 6s states at the bottom of the conduction band vanish causing additional widening of the band gap. Further, our calculation suggests that the $Ba_2PrPr_{Bi}O_6$ is a possible candidate as a source of the Pr^{IV} signal observed in the experiment. We find that the *B*-site disorder atomic configurations, $Ba_2B''^{V}B'^{III}O_6$, are easily restored to those of the original structures. This demonstrates the stability of the *B*-site ordering in the double-perovskite framework. On the other hand, our results also suggest the importance of the partial *B*-site disorder in the double-perovskites to explain the experimentally observed band gaps.

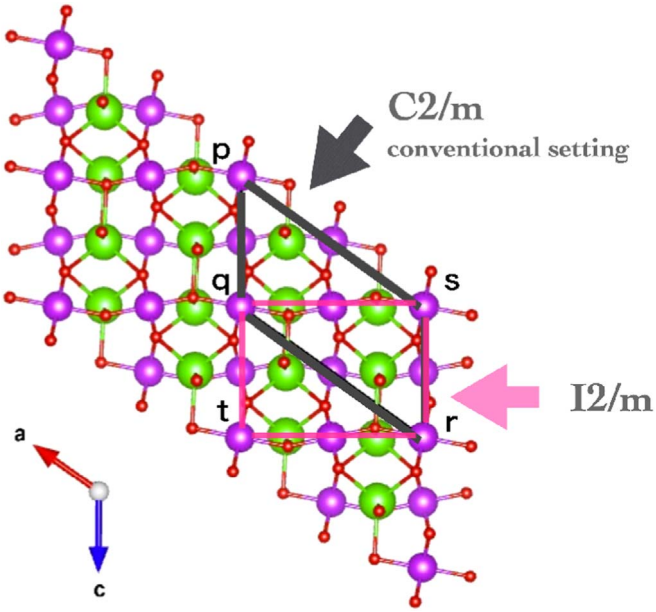

Figure 1. $Ba_2Bi^{III}Bi^{V}O_6$ with the $C2/m$ symmetry projected on the (010) plane. Bi (Ba) atoms are large dark-purple (light-green) spheres. Small spheres are the oxygen atoms. A $C2/m$ unit cell contains four $BaBiO_3$ chemical units and is the region indicated with the letters p, q, r, and s, while an $I2/m$ unit cell is the region indicated with the letters q, t, r, and s.

2. Calculation method

We use the density functional theory (DFT) as implemented in the Vienna ab-initio Simulation Package (VASP) [12] and the projector augmented wave (PAW) potentials [13] to study the structural and electronic properties of the double perovskite. It has been known that standard exchange-correlation functionals, such as the local density approximation (LDA) and the generalized gradient approximation (GGA), predict the electronic properties of double perovskites as metal or semi-metal with a very narrow band gap [14]. Theoretical study considering the electron correlations through the GGA+U method showed an improvement on the optimized structural and electronic properties of $Ba_2Bi^{III}Bi^{V}O_6$ [15]. However, since the method utilizes specially tuned parameter U, application of the method to the other double-perovskites is not straightforward. On the other hand, recently developed Heyd-Scuseria-Ernzerhof hybrid functional (HSE06) [16, 17] is known to have an ability to account for the strong correlation effects and has been successfully applied to analyze the structural and electronic properties of the double-perovskites [18]. Therefore we use the HSE06 functional throughout our study. We use an energy cutoff of 500eV for plane wave basis set together with a $6 \times 6 \times 6$ **k**-point grid. The rather high energy cutoff and dense **k**-point grid are necessary to predict correctly the crystal structures in the HSE06 computations. Equilibrium crystal structures were achieved so that the maximum force component was smaller than 1 meV/Å^3, and the maximum stress component smaller than 1 meV/Å^3. Optimized crystal structures were visualized using the VESTA [19].

3. Results and discussion

First of all, we evaluate the structural and electronic properties of $Ba_2Bi^{III}Bi^{V}O_6$ as it gives the basis in analyzing the double perovskite crystals [20, 21]. Unit cell contains four $BaBiO_3$ chemical units where the Bi^{III} octahedra and the Bi^{V} octahedra are arranged alternately forming the B-site ordering. It has the monoclinic $I2/m$ symmetry at room temperature [22], and which is equivalent to the conventional setting of $C2/m$ No.12 [23, 24]. The $I2/m$ cell is outlined on the $C2/m$ supercell in the figure 1.

Where the distortions of octahedra caused by the mixed valencies are characterized by breathing distortion δ and tilting angle ϕ as depicted in figure 2.

Structural optimization has been done for the room temperature phase of $C2/m$ (table 1). Lattice constants optimized within PBE are significantly overestimated thereby causing the overestimation of v_0. On the other hand, HSE06 correctly predicts not only the lattice constants but also the internal distortion parameters, δ and ϕ. The difference is even clear when we calculate the electronic property of the system: $Ba_2Bi^{III}Bi^{V}O_6$ is semi-metallic in the PBE functional while it opens band gap significantly when we use the HSE06 functional consisting

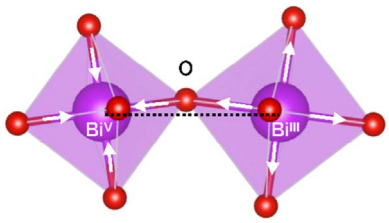

Figure 2. Distorted octahedra of $Ba_2Bi^{III}Bi^{V}O_6$. Where ϕ is defined as the average tilting angle of the neighboring $Bi^{III}O_6$ and $Bi^{V}O_6$ from the dotted line which is equal to the c-axis of the $I2/m$ cell. $\delta = \frac{1}{2}(\overline{Bi^{III}O} - \overline{Bi^{V}O})$ is defined as the breathing distortion, with $\overline{Bi^{III}O}$ and $\overline{Bi^{V}O}$ are average Bi^{III}-O and Bi^{V}-O distances, respectively [14].

Table 1. Structural parameters of $Ba_2Bi^{III}Bi^{V}O_6$. Lattice parameters (a, b, and c) and the angle β in the monoclinic $I2/m$ cell extrapolated from those of the $C2/m$ cell are presented. Cell volume per chemical formula unit is v_0. δ and ϕ are the breathing distortion and the tilting angle, respectively.

	a (Å)	b (Å)	c (Å)	β (deg)	v_0 (Å^3)	δ (Å)	ϕ (deg)
HSE06 (This work)	6.201	6.150	8.681	90.35	82.77	0.10	11.1
PBE (This work)	6.276	6.228	8.793	90.27	85.93	0.14	12.4
HSE06[a]	⋯	⋯	⋯	90.24	82.10	0.09	11.9
PBE[a]	⋯	⋯	⋯	90.16	85.76	0.07	12.1
Exp1[b]	6.1814	6.1360	8.6697	90.173	82.21	0.085	11.2
Exp2[c]	6.1908	6.1450	8.6785	90.164	82.54	0.166	9.43
Exp3[d]	6.1851	6.1322	8.6585	90.229	82.10	0.180	10.30

[a] Values were calculated in the optimized structure derived from the cubic high temperature phase ($Fm\bar{3}m$) [14].

[b] Experimental data at room temperature [21].

[c] Experimental data at 295 K [26].

[d] Experimental data at 200 K [22].

with the experiment. It has been argued that this shortcoming of the PBE comes from lesser ability in describing the exchange correlation effect of strongly-correlated electron system [18, 25].

Next, we calculate the electronic band structure. In a monoclinic system, the shape of the Brillouin zone depends non-trivially on the lattice vectors [27]. In fact, there are five possible shapes of Brillouin zones for the monoclinic crystal structure depending on the choice of lattice vectors [28, 29]. We choose the $C2/m$ which corresponds to the $MCLC_1$ lattice as defined in [29]. To generate the set of **k**-points along the edges of the Brillouin zone, we use the code pymatgen [30].

High resolution band structures and electronic density of states curves were obtained thorough the WANNIER90 package by constructing maximally localized Wannier functions (MLWFs) [31–34] using the VASP2WANNIER90 interface [35] (figure 3). The band gap is indirect and $E_i(\mathrm{L} \rightarrow \mathrm{Z}) = 0.84$ eV while the direct band gap is $E_d = 2.02$ eV. Electron distributions of the valence band maximum (VBM) and of the conduction band minimum (CBM) evaluated at the Γ point are shown in the figure 4. We can see the 6s electrons of Bi^{III} and the O 2p electrons at the VBM state (Figure 4(a)) reflecting their valence states while the 6s electrons of Bi^{V} are visible at the CBM state (figure 4(b)).

We substituted Pr for the Bi^{III} to form Ba_2PrBiO_6. The optimized structural parameters show an excellent agreement with the experiments (table 2). Electronic band structure is given in the figure 5. The band gap is indirect $E_i(\mathrm{Z} \rightarrow \Gamma) = 3.58$ eV and the direct band gap is $E_d = 3.70$ eV. It is visible that the two isolated valence bands near the fermi level are now vanished. The breathing distortion δ as well as the tilting angle ϕ retain the values before the substitution reflecting the preservation of their valence states ($Ba_2Pr^{III}Bi^{V}O_6$).

It has been reported that experimentally prepared Ba_2PrBiO_6 sample exhibits the valence mixing between Pr^{III} and Pr^{IV} [10, 11]. In the experiment, the valence state Pr^{IV} was gradually suppressed as the amount of substitution of Sb for Bi was increased, and was completely resolved in the $Ba_2Pr^{III}Sb^{V}O_6$ sample. However, the valence state Pr^{IV} must be compensated locally to keep the charge neutrality. One of the potential candidates for the compensation is the locally generated B-site disorder. We construct the structure by exchanging the atomic positions of Pr and Bi ($Ba_2Pr^{III}Bi^{V}O_6 \rightarrow Ba_2Bi^{III}Pr^{V}O_6$) while fixing the framework made by Ba and O atoms.

After the optimization, the structure recovered to that of the $Ba_2Pr^{III}Bi^{V}O_6$ by adjusting the distances from Pr and Bi to the nearest oxygen atoms and the valence state Pr^{IV} was not be realized. Next, we investigated the

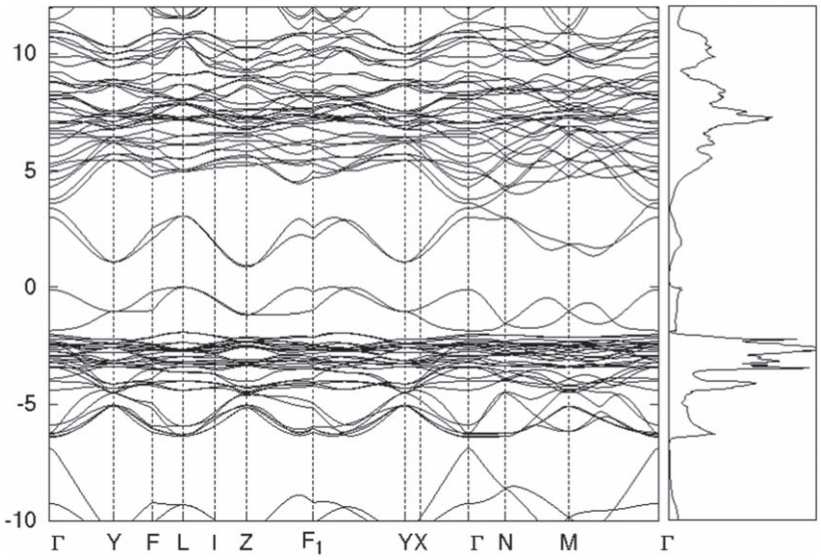

Figure 3. Band structure and density of states curve of $Ba_2Bi^{III}Bi^{V}O_6$. Fermi level is at 0 eV.

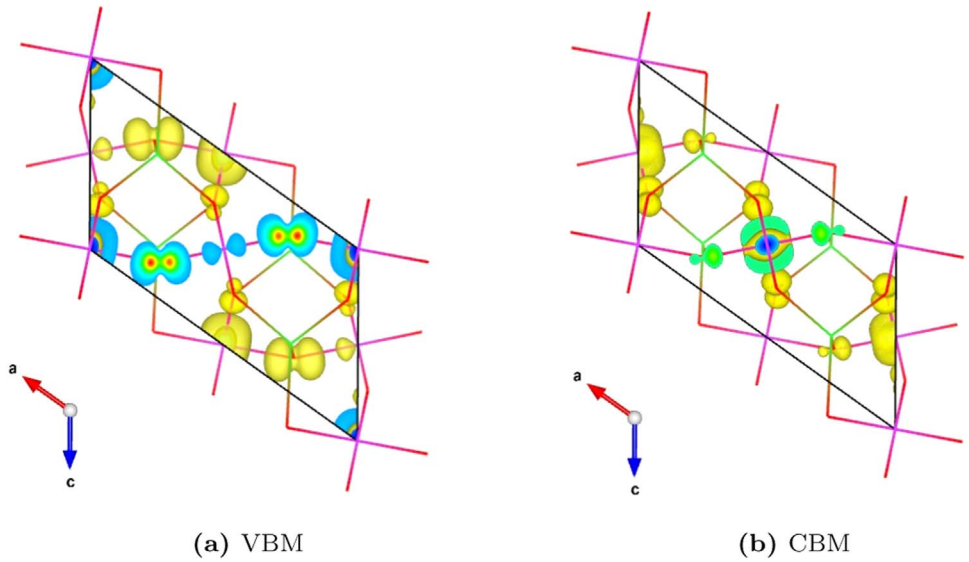

Figure 4. The Bi^{III} 6s orbitals are visible at the middle points of the upper and lower sides, and at the four corners of the cell in the VBM charge density distribution (a) while those of Bi^{V} appear at the middle points of left and right sides, and at the center of the cell in the CBM charge density distribution (b). The wire-frame representation for the $C2/m$ atomic arrangements (figure 1) is used to improve the visibility. Where some of the orbitals are showing their sections at the boundaries of the unit cell.

Table 2. Structural parameters of Ba_2PrBiO_6. The same notations for columns of the table 1 are used.

	a (Å)	b (Å)	c (Å)	β (deg)	v_0 (Å^3)	δ (Å)	ϕ (deg)
This work.	6.211	6.169	8.707	90.41	83.41	0.12	11.1
Exp1[a]	6.204	6.169	8.701	90.27	83.20		
Exp2[b]	6.201	6.158	8.697	90.08	83.03		

[a] Reference [11].
[b] Reference [23].

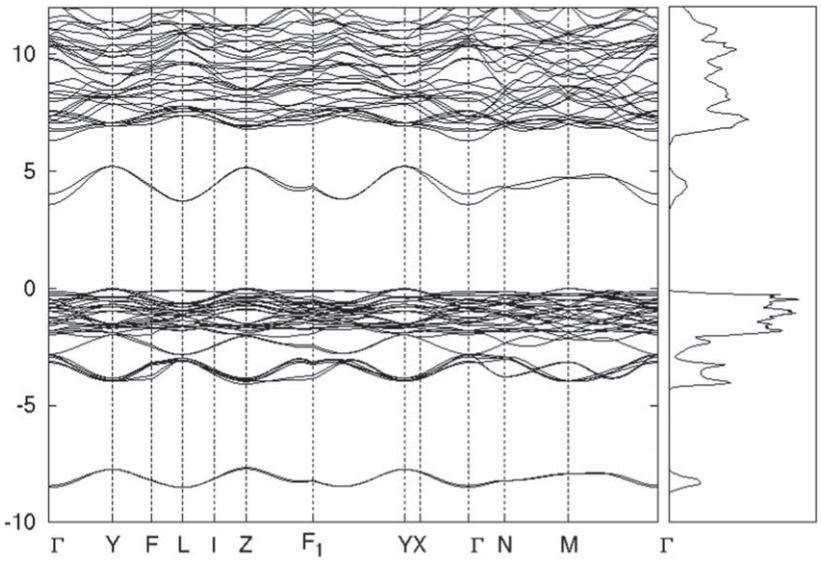

Figure 5. Band structure and density of states curve of $Ba_2Pr^{III}Bi^{V}O_6$. Two isolated valence bands near the Fermi level of $Ba_2Bi^{III}Bi^{V}O_6$ were vanished due to the B'^{III}-site substitution.

Table 3. Structural parameters of Ba_2PrSbO_6. The same notations for columns of the table 1 are used.

	a (Å)	α (deg)	v_0 (Å^3)	δ (Å)	ϕ (deg)
This work.	6.075	60.00	78.65	0.16	6.5
Expt.[a]	6.047	60.16	78.64		

[a] Experimental value [11].

substitution defect of Pr_{Bi} to see if the B-site ordering is preserved by forming the $Ba_2Pr^{III}Pr^{V}_{Bi}O_6$. After the structural optimization, all the distances between Pr and neighboring oxygen atoms became to be 2.33 Å ($\delta = 0$) as the result of the single valency formation of $Pr^{IV}(Ba_2Pr^{IV}Pr^{IV}_{Bi}O_6)Pr$. It has a similar structural feature of the cubic $BaPr^{IV}O_3$ (high temperature phase, space group $Pm\bar{3}m$) [36] except the rather elongated Pr-O bond length and the residual tilting angles. We found that the total energy of $Ba_2PrPr_{Bi}O_6$ per $BaPrO_3$ chemical unit is lower than that of the cubic $BaPrO_3$. Our calculation suggests that the $Ba_2PrPr_{Bi}O_6$ is a possible candidate as a source of the Pr^{IV} signal observed in the experiment, where the residual Bi may contribute to form $Ba_2Bi^{III}Bi^{V}O_6$.

We now focus on the substitution of the smaller ion Sb^{V} for Bi^{V}. The stable crystal structure is $R\bar{3}$. Again, the optimized crystal structure shows excellent agreement with the experimental one (table 3).

The distances from Pr and Sb to the nearest neighbor oxygen atoms are almost identical to those of the Ba_2PrBiO_6, reflecting the formation of the valence state of $Ba_2Pr^{III}Sb^{V}O_6$. We also tried to create the B-site disordered structure by interchanging the atomic positions of Pr and Sb in Ba_2PrSbO_6. Structural optimizations were performed only for the atomic positions while fixing the cell shape and the cell volume. The system again restores its crystal symmetry demonstrating the stability of the B-site ordering of the $Ba_2Pr^{III}Sb^{V}O_6$ framework.

The electronic band structure is shown in the figure 6. The Bi^{V} bands located at the bottom of the conduction bands of $Ba_2Pr^{III}Bi^{V}O_6$ are vanished and the band gap is widened. The calculated indirect band gap is $E_i(Z \rightarrow L) = 5.90$ eV and the direct band gap is $E_d = 5.97$ eV. Experimentally estimated band gap E_{ex} also show the similar widening tendency on the substitution of Sb for Bi^{V} ($E_{ex}(Ba_2PrBiO_6) = 0.977$ eV $\rightarrow$ E_{ex} $(Ba_2PrSbO_6) = 2.395$ eV [11]). However, the experimental values are about half of the theoretical values obtained in this work.

The hybrid functional HSE06 incorporates the short-range Hartree–Fock type exchange at the fraction of α ($0 < \alpha < 1$). It has been reported that the parameter α is somewhat material-specific and the best value often deviates from the standard value of $\alpha = 0.25$ [18, 27, 35]. Therefore we calculated the band gaps for $\alpha = 0.25$, 0.1, and 0.05 to see if it is the case for the double-perovskites (table 4).

The band gaps of $Ba_2Bi^{III}Bi^{V}O_6$ calculated with the small α significantly deviate from the experimental ones while those of the $Ba_2Pr^{III}Bi^{V}O_6$ and $Ba_2Pr^{III}Sb^{V}O_6$ show decreasing tendency with decreasing the α but are still lager than the experimental values. We can conclude that the adoption of the smaller α does not improve the

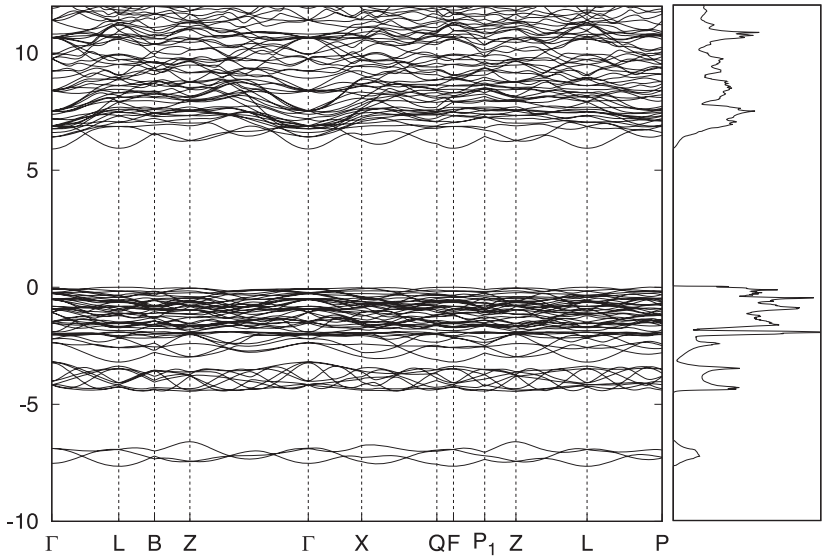

Figure 6. Band structure and density of states curve of $Ba_2Pr^{III}Sb^{V}O_6$. Two isolated conduction bands near the Fermi level of $Ba_2Pr^{III}Bi^{V}O_6$ were vanished due to the B''^{V}-site substitution.

Table 4. HSE06 band gaps (eV) calculated for the $\alpha = 0.25, 0.1$, and 0.005. Experimental band gaps are also shown (Expt.). Band gaps of *B*-site disordered double-perovskites, Ba_2 $(Pr^{III} \leftrightarrow Bi^{V})O_6$ and Ba_2 $(Pr^{III} \leftrightarrow Sb^{V})O_6$ without structural relaxations, are also shown.

	HSE06						Expt.	
	$\alpha = 0.25$[a]		$\alpha = 0.1$		$\alpha = 0.05$			
	E_d	E_i	E_d	E_i	E_d	E_i	E_d	E_i
$Ba_2Bi^{III}Bi^{V}O_6$	2.02	0.84	1.55	0.50	1.40	0.39	2.0[b,c]	0.2[c]
	2.07[d]	0.84[d]						
$Ba_2Pr^{III}Bi^{V}O_6$	3.70	3.58	2.82	2.77	2.54	2.50		0.977[e]
Ba_2 $(Pr^{III} \leftrightarrow Bi^{V})O_6$	1.14	0.78						
$Ba_2Pr^{III}Sb^{V}O_6$	5.97	5.90	4.94	4.90	4.61	4.55	2.395[e]	
Ba_2 $(Pr^{III} \leftrightarrow Sb^{V})O_6$	1.89	1.09						

[a] Standard value used in the HSE06 calculation.
[b] Reference [37].
[c] Reference [38].
[d] Reference [14].
[e] Reference [11].

disparity of the band gaps. On the other hand, we focus on the partial disorder of the *B*-sites as it has been experimentally found in the $Ba_2Pr^{III}Bi^{V}O_6$ sample [23]. Although our calculation indicates that the *B*-site disordered double-perovskites are energetically unfavorable, it dose not exclude the possibility of the presence of partial disordered *B*-sites in the ordered double-perovskite matrices. It is well known that the electronic properties of semiconductors are easily modified significantly by incorporation of small amounts of impurities or other kind of defects [39]. We evaluated the band gaps of the *B*-site disordered double-peroveskites using the standard value for the α (table 4). Structural relaxations were not performed. We found fluctuating behavior both in the lowest conduction band and the highest valence band thereby significantly narrowing their band gaps. The indirect band gap of the *B*-site disordered $Ba_2Pr^{III}Bi^{V}O_6$ is $E_i = 0.78$ eV which is comparable to the experimental value of 0.977eV. Similarly, the direct band gap of the *B*-site disordered $Ba_2Pr^{III}Sb^{V}O_6$ is $E_d = 1.89$ eV which is also comparable to the experimental value of 2.395 eV. Although the *B*-site disordering of the $Ba_2Pr^{III}Sb^{V}O_6$ has not been observed in the experiments yet, our results indicate that the *B*-site disordering atomic configurations in the double-perovskites may control their band gaps.

4. Conclusion

Density functional calculations were performed to investigate the structural and electronic properties of the double-perovskites, $Ba_2Bi^{III}Bi^{V}O_6$, Ba_2PrBiO_6, and Ba_2PrSbO_6. The *B*-site ordering in the $Ba_2Bi^{III}Bi^{V}O_6$ creates typical electronic band structure, where the top of the valence bands are composed of Bi^{III} 6s orbitals while the bottom of the conduction bands are composed of Bi^{V} 6s orbitals. By substituting the Pr for Bi^{III}, two valence band originated in the Bi^{III} 6s orbitals are vanished thereby widening the band gaps. Substitution of Sb for Bi^{V} induces additional band gap widening. Further, our calculation suggests that the $Ba_2PrPr_{Bi}O_6$ is a possible candidate as a source of the Pr^{IV} signal observed in the experiment. The *B*-site disordering atomic configurations are restored to those of the original crystal structures. It demonstrates the stability of the *B*-site ordering in the double-perovskite framework. However, it does not exclude the presence of the partial *B*-site disordering as it has been experimentally observed in the $Ba_2Pr^{III}Bi^{V}O_6$ sample. Calculated band gaps for the *B*-site disordered $Ba_2Pr^{III}Bi^{V}O_6$ and $Ba_2Pr^{III}Sb^{V}O_6$ show comparable results with the experiments. Although the *B*-site disordering of the $Ba_2Pr^{III}Sb^{V}O_6$ has not been observed in the experiments yet, our results indicate that the *B*-site disordered atomic configurations in the double-perovskites may play an important role to adjust their band gaps.

Acknowledgments

This work was supported in part by JSPS KAKENHI Grant No. JP19K04995, Iketani Science and Technology Foundation, and The Mazda Foundation. The authors thank the Iwate University Super-Computing and Information Sciences Center, the Cyberscience Center, Tohoku University, and the Supercomputer Center of the Institute for Solid State Physics, University of Tokyo, for providing the computational resources.

ORCID iDs

Kazume Nishidate https://orcid.org/0000-0002-3003-4020
Haruka Taniguchi https://orcid.org/0000-0002-9739-4047

References

[1] Fujishima A and Honda K 1972 *Nature* **238** 37
[2] Hoffmann M R, Martin S T, Choi W and Bahnemann D W 1995 *Chem. Rev.* **95** 69
[3] Ohko Y, Tryk D A, Hashimoto K and Fujishima A 1998 *J. Phys. Chem.* B **102** 2699
[4] Zou Z, Ye J, Sayama K and Arakawa H 2001 *Nature* **414** 625
[5] Karkmaz M, Puzenat E, Guillard C and Herrmann J 2004 *J. M. Appl. Catal.* B **51** 183
[6] Zhu H, Lan Y, Gao X, Ringer S P, Zheng Z, Song D and Zhao J 2005 *J. Am. Chem. Soc.* **127** 6730
[7] Vasala S and Karppinen M 2015 *Prog. in Solid State Chem.* **43** 1
[8] Hatakeyama T, Takeda S, Ishikawa F, Ohmura A, Nakayama A, Yamada Y, Matsushita A and Yea J 2010 *J. Cer. Soc. Jpn.* **118** 91
[9] Matsushita A, Nakane A, Naka T, Isago T and Yamada H 2012 *Jpn. J. Appl. Phys.* **51** 121802
[10] Onodera K, Kogawa T, Matsukawa M, Taniguchi H, Nishidate K, Matsushita A and Shimoda M 2018 *J. Phys. Conf. Ser.* **969** 012122
[11] Taniguchi H, Matsukawa M, Onodera K, Nishidate K and Matsushita A 2019 *IEEE Trans. on Mag.* **55** 2400404
[12] Kresse G and Furthmüller J 1996 *Phys. Rev.* B **54** 11169
[13] Blöchl P 1994 *Phys. Rev.* B **50** 17953
[14] Franchini C, Sanna A, Marsman M and Kresse G 2010 *Phys. Rev.* B **81** 085213
[15] Korotin D, Kukolev V, Kozhevnikov A V, Novoselov D and Anisimov V I 2012 *J. Phys., Condens. Matt.* **24** 415603
[16] Heyd J, Scuseria G E and Ernzerhof M 2003 *J. Chem. Phys.* **118** 8207
[17] Heyd J, Scuseria G E and Ernzerhof M 2006 *J. Chem. Phys.* **124** 219906
[18] Franchini C 2014 *J. Phys. Condens. Matter* **26** 253202
[19] Momma K and Izumi F 2011 *J. Appl. Crystallogr.* **44** 1272
[20] Cox D E and Sleight A W 1976 *Solid State Commun.* **19** 969
[21] Cox D E and Sleight A W 1979 *Acta Crystallogr. Sect. B: Struct. Crystallogr. Cryst. Chem.* **35** 1
[22] Kennedy B J, Howard C J, Knight K S, Zhan Z and Zhau Q 2006 *Acta Cryst.* B **62** 537
[23] Harrison W T A, Reis K P, Jacobson A J, Schneemeyer L F and Waszczak J V 1995 *Chem, Mater* **7** 2161
[24] Jaffe H W 1996 *Crystal Chemistry and Refractivity* (Mineola, New York: Dover Publications, Inc.) 220–1
[25] Smolyanyuk A, Boeri L and Franchini C 2017 *Phys. Rev.* B **96** 035103
[26] Pei S, Jorgensen J D, Dabrowski B, Hinks D G, Richards D R, Mitchell A W, Newsam J M, Sinha S K, Vaknin D and Jacobson A J 1990 *Phys. Rev.* B **41** 4126
[27] Peelaes H and van de Walle C G 2015 *Phys. Status Solidi* B **252** 828
[28] Ruzaikin M P and Kudryavtseva N V 1974 *Russ. Phys.* J **17** 934
[29] Setyawan W and Curtarolo S 2010 *Comput. Mater. Sci.* **49** 299
[30] Ong S P, Richards W D, Jain A, Hautier G, Kocher M, Cholia S, Gunter D, Chevrier V, Persson K A and Ceder G 2013 *Comp. Mat. Sci.* **68** 314
[31] Mostofi A A, Yates J R, Lee Y-S, Souza I, Vanderbilt D and Marzari N 2008 *Comput. Phys. Commun.* **178** 685

[32] Marzari N and Vanderbilt D 1997 *Phys. Rev.* B **56** 12847
[33] Souza I, Marzari N and Vanderbilt D 2001 *Phys. Rev.* B **65** 035109
[34] Marzari N, Mostofi A A, Yates J R, Souza I and Vanderbilt D 2012 *Rev. Mod. Phys.* **84** 1419
[35] Franchini C, Kováčik R, Marsman M, Murthy S S, He J, Ederer C and Kresse G 2012 *J. Phys.: Condens. Matt.* **24** 235602
[36] Saines P J, Kennedy B J and Smith R I 2009 *Mat. Res. Bull.* **44** 874
[37] Uchida S, Kitazawa K and Tanaka S 1987 *Phase Transitions* **8** 95
[38] Kim K H, Jung C U, Noh T W and Kim S C 1997 *Phys. Rev.* B **55** 15393
[39] Yu P Y and Cardona M 2005 *Fundamentals of Semiconductors* 3rd edn. (Berlin: Springer) pp. 159–202